

# Preliminary Results on Energy Efficient 3D Prosthetic Walking with a Powered Compliant Transfemoral Prosthesis

Huihua Zhao<sup>1</sup>, Eric Ambrose<sup>2</sup> and Aaron D. Ames<sup>3</sup>

**Abstract**—This work presents the preliminary experimental validation of a systematic prosthetic control strategy on a custom compliant transfemoral prosthesis with the end result being energy efficient 3-dimension (3D) multi-contact prosthetic walking. In particular, with the goal of capturing essential components of realistic amputee-prosthesis system, a 3D asymmetric hybrid system model is presented—this forms the foundation for formal gait design and control construction. Based on this model, a two-step direct collocation optimization method is utilized to design an energy efficient multi-contact prosthetic gait in 3D. The designed gaits are also subject to various practical constraints such as human-likeness constraints and comfortability constraints. For experimental validation, a 3D capable powered transfemoral prosthetic device is custom built so as to be amendable to realizing the designed 3D prosthetic gaits. Differentiating this device from existing powered prostheses, compliant components are added to the three joints (two pitch joints and one roll joint) for the purpose of energy saving and human-like behaviors. Combining the presented control methodology and the novel hardware design, the end result is experimentally realized 3D multi-contact prosthetic walking with improved energy efficiency compared to other devices and control methods.

## I. INTRODUCTION

There are approximately 1.9 million people in the United States alone that are living with limb loss, and this number is expected to double by the year 2050 [36]. Despite this large demographic, the current market for commercial prostheses remains largely limited to energetically passive prosthetic devices, limiting the day-to-day life of amputees [9], [31]. Powered-lower-limb prostheses capable of providing net power in conjunction with various prosthetic controllers have been developed with the potential to regain full mobility in various terrains for amputees. Additionally, with intelligent high-level motion planning controllers, active prostheses also have the potential to increase self-selected gait speed and gait symmetry while reducing metabolic cost and wear-and-tear on the amputees' unaffected joints [29].

While these potential benefits are compelling from various perspectives, there still remains many challenges such as mechanical design, system modeling, control development,

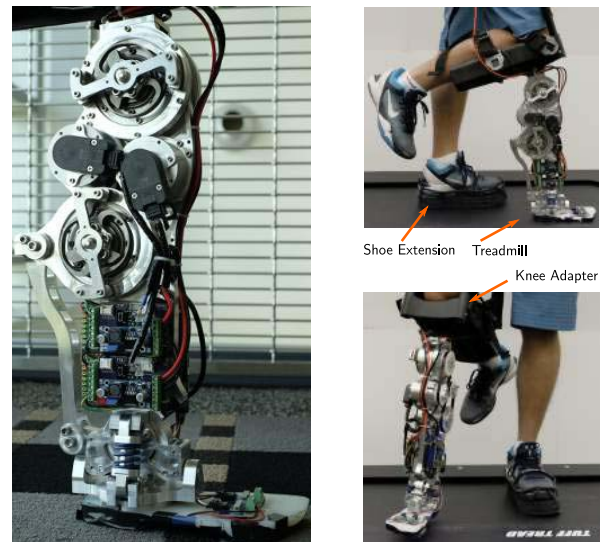


Fig. 1: Assembled hardware of AMPRO3 (left) and the experimental testing setup (right).

and human-device interaction [29]. In particular, the prosthetic devices must be as compact and light as possible while still able to mechanically provide enough torque to bear human weight. Proper compliance is also necessary to mimic human tendon for the purpose of energy saving and comfortability [31]. A systematic way of designing and validating control approaches is necessary in order to develop prosthetic controllers that can be generalized to different devices or amputees. Motivated by these problems, this paper takes the first steps of answering these challenges via a systematic control framework (for generating formal 3D prosthetic gaits) and a novel powered prosthetic device (with 3D capability and compliant joints).

Among various prosthetic controllers, variable impedance control is one of the most common approaches for controlling prostheses (to name a few [5], [17], [26], [27]). With breaking one step cycle into multiple phases, this controller requires clinical tuning of these control parameters for each patient [27]. Moreover, multiple sessions are necessary to tune the devices for different modes of locomotion. On the other end of the spectrum, as motivated by the control of bipedal robotic research, virtual constraints can be utilized to design a unified reference prosthetic gait for tracking purpose [6], [11], [14], [35]. Compared to the traditional impedance

\*This research is supported by the funding NRI-1526519.

<sup>1</sup>H. Zhao has graduated from the AMBER Lab and now is with SRI Robotics, Menlo Park, CA, USA huihua.zhao@sri.com

<sup>2</sup>E. Ambrose is with Mechanical Engineering, California Institute of Technology, Pasadena, CA, USA. eambrose@caltech.edu

<sup>3</sup>Prof. A. Ames is with department of Mechanical and Civil Engineering, California Institute of Technology, Pasadena, CA, USA. ames@cds.caltech.edu

control, this method presents advantages such as no step discretization required, formal stability analysis and the possibility of implementing optimal nonlinear controllers.

Previous work of the authors have proposed a systematic methodology—including optimization and nonlinear control—for realizing 2D prosthetic walking of AMPRO1 with achieving reduced parameter tuning and improved energy efficiency [34], [35]. To further validate this systematic methodology for more practical situation, this paper considers a 3D asymmetrical amputee-prosthesis hybrid system model for more realistic prosthetic gaits design. Specific requirements—such as amputee comfortability and human-likeness—are considered in order to generate a well-designed prosthetic gait. More importantly, as the first main contribution of this work, a passive compliant ankle roll joint is considered for the prosthetic side in the modeling. Leveraging a computation efficient two-step direct collocation optimization method [15], in the framework of which both the hybrid zero dynamics constraints and the prosthetic gait requirements can be imposed as explicit nonlinear constraints, an energy optimal 3D multi-contact prosthetic gait is generated automatically. The control Lyapunov function based nonlinear controller is then introduced briefly to optimally realize the designed gait on the hardware.

Another major challenge in the development of a powered prosthesis is that the devices require both high power to weight ratio (power density) and energy to weight ratio (energy density) [16]. Springs, which can be viewed as robotic tendons, have been a natural choice in prosthetic and orthotic technologies for purposes such as peak torque shift, better terrain adaption [8], [28] and energy storage and return [20], [23]. However, most of these work are limited either to passive devices or active devices with only one joint powered and in 2D case. With the beneficial aspects of compliance as motivation, another main contribution of this work is to propose the creation of a novel 3D transfemoral prosthesis: AMPRO3 with compliance being added to all three joints. In particular, two series elastic actuators (SEA) are used for both ankle and knee pitch joints, which allows for energy saving possibilities. A novel passive ankle roll joint with springs is added to the design specifically for adding user comfortability and mobility. The on-board sensing and computation are presented to give a complete design overview.

The preliminary experiment results of AMPRO3 are discussed in this paper, indicating that the proposed framework can be successfully extended to the 3D case. More importantly, with achieving natural human-like foot behavior and energy saving, the systematic method—from formal modeling, to gait generation, nonlinear control and novel hardware design—has a promising potential to improve the everyday lives of amputee patients.

## II. CONTROL METHOD

This section briefly introduces the systematic method—including hybrid system modeling, virtual constraints based control law and gait design optimization—for realizing 3D

multi-contact prosthetic walking. More detailed discussion can be referred to in [32].

### A. MODELING OF AMPUTEE-PROSTHESIS SYSTEM

1) *Multi-Domain Hybrid System Model*: Human locomotion encompasses a cyclic pattern with domains (including both continuous dynamics and discrete dynamics) transitioning in an ordered and periodic manner. This motivates the use of a multi-domain hybrid system with a predetermined ordering of phases (or domains) as represented by a cyclic directed graph [4], [33]. Formally, the definition of a *multi-domain hybrid control system* is given as a tuple,

$$\mathcal{HC} = (\Gamma, \mathcal{D}, \mathcal{U}, S, \Delta, FG), \quad (1)$$

where  $\Gamma = (V, E)$  is a directed cycle. For space limitation, we put a special focus on the continuous dynamic of the hybrid system model with omitting the rest of the elements. More details can be found in [4], [32], [33].

2) *Dynamics of Amputee-Prosthesis System*: From a mathematical modeling perspective, an amputee-prosthesis system is an asymmetric system with each leg having different properties in various aspects (for example, mass and inertia properties). The number of actuated joints and feasible torques may also be different. These differences require us to model the amputee part and prosthetic leg as sub-systems separately. Holonomic constraints will be then utilized to combine these two sub-systems into a single complete bipedal robotic system.

**Continuous Dynamics of Sub-Systems.** Both the amputee (or human) and the prosthesis sub-systems can be modeled as a kinematic chain along with holonomic constraints. For the amputee sub-system, an inertial reference frame  $R_b = \{p_b, \phi_b\} \subset \mathbb{R}^6$  is defined at the center of the hip as shown in Fig. 2. As illustrated in the left plot of Fig. 2, the kinematic chain of whole body coordinates consists of three branches: waist joints  $q_w = [\psi_w, \phi_w, \theta_w]^T$ , left leg (which is assumed to be the unimpaired leg) joints  $q_l = [\psi_{lh}, \phi_{lh}, \theta_{lh}, \theta_{lk}, \theta_{la}, \phi_{la}, r_{ls}]^T$  and the right amputated hip  $q_{rh} = [\psi_{rh}, \phi_{rh}, \theta_{rh}]^T$ , respectively. Therefore, the configuration space of the human sub-system is defined as  $\mathcal{Q}_h : q_h = \{R_b, q_w, q_l, q_{rh}\} \subset \mathbb{R}^{19}$  with 13 degrees of actuation (6 actuators at the two hips, 3 at the waist, 1 at the knee and 2 at the ankle). Similarly, considering the fact that the prosthetic device will be connected to the amputee at the right amputated thigh by using a socket adapter, we choose base frame for prosthesis leg  $R_s = \{p_s, \phi_s\} \subset \mathbb{R}^6$  at the place where the socket adapter is, which is shown as the green block in Fig. 2. The prosthetic leg has 4 degrees of freedom  $q_{rp} = [\theta_{rk}, \theta_{ra}, \phi_{ra}, r_{rs}]^T$  and is actuated only at the joints of knee and ankle pitch. Note that, the rubber shoes are modeled as stiff passive springs to better capture the compliance characteristics the sole. The spring constants are determined based on the result in [13]. During the modeling process, the springs are considered as “actuated joints”, however, with constrained control input  $u = k_p r + k_d \dot{r}$ , where  $r$ ,  $\dot{r}$ ,  $k_p$  and  $k_d$  are the displacement, velocity, spring constant and damping of the springs, respectively.

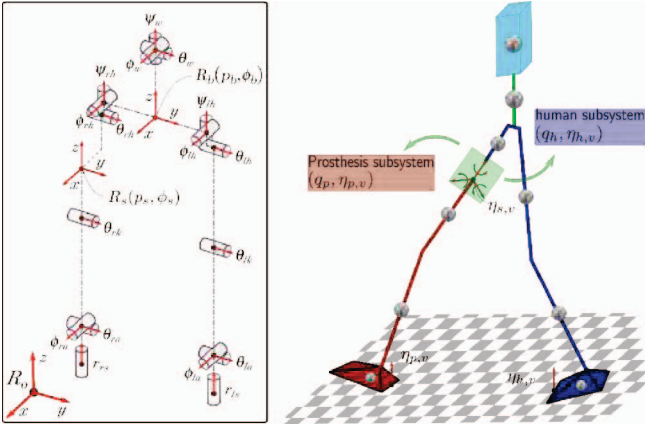


Fig. 2: Model of amputee-prosthesis system.

With the anthropomorphic mass, inertia and length properties of each link estimated based on the method in [31] of a real testing subject, the equation of motion for a given domain  $\mathcal{D}_v$  of the amputee sub-system is determined by the Euler-Lagrange equation [12], [21]:

$$D_h(q_h)\ddot{q}_h + H_h(q_h, \dot{q}_h) = B_{h,v}u_{h,v} + J_{h,v}^T(q_h)F_{h,v}, \quad (2)$$

where  $F_{h,v} : T\mathcal{Q}_h \times U_{h,v} \rightarrow \mathbb{R}^{n_{h,v}}$ , with  $n_{h,v}$  the number of total holonomic constraints, is a vector of contact wrenches containing the constraint forces and/or moments (see [21]).  $J_{h,v}$  is the corresponding Jacobian matrix of the contact points (i.e., holonomic constraints set denoted as  $\eta_{h,v}$ ) of the amputee in domain  $v$ . To enforce the holonomic constraints, the second order differentiation of the constraints,  $\eta_{h,v}$  should be set to zero, i.e.,  $J_{h,v}(q_h)\ddot{q}_h + \dot{J}_{h,v}(q_h, \dot{q}_h)\dot{q}_h = 0$ . Similarly, the constrained dynamics of the prosthesis sub-system can also be derived by replacing the corresponding terms respectively (see [32]).

Note that, differentiating from the modeling in [32], this work adds a compliant ankle roll joint for modeling of the prosthesis sub-system, which is based on the mechanical design that will be presented later. While this actuation asymmetry (since human ankle roll joint is actuated) adds significant difficulty to the gait design process, it yields a more realistic model for the purpose of better gait generation.

**Combined Bipedal Amputee-Prosthesis System.** For the combined bipedal system, the configuration space can be defined as  $\mathcal{Q} : q = \{q_h, q_p\} \subset \mathbb{R}^{29}$ ; holonomic constraints are grouped as  $\eta_v = \{\eta_{h,v}, \eta_{p,v}, \eta_{s,v}\}$  (corresponding to  $F_v = \{F_{h,v}, F_{p,v}, F_{s,v}\}$ ) where  $\eta_{s,v}$  ( $F_{s,v}$ ) is the set of holonomic constraints imposed by the socket. Therefore, the general dynamics for  $\mathcal{D}_v$  can be given as:

$$D(q)\ddot{q} + H(q, \dot{q}) = B_v u_v + J_v^T(q)F_v, \quad (3)$$

$$J_v(q)\ddot{q} + \dot{J}_v(q, \dot{q})\dot{q} = 0. \quad (4)$$

Due to this asymmetric model construction, one human stance step (HS) and one prosthesis stance step (PS) are necessary to form a complete two-step multi-contact cycle, resulting in a directed graph with 8 domains as shown in

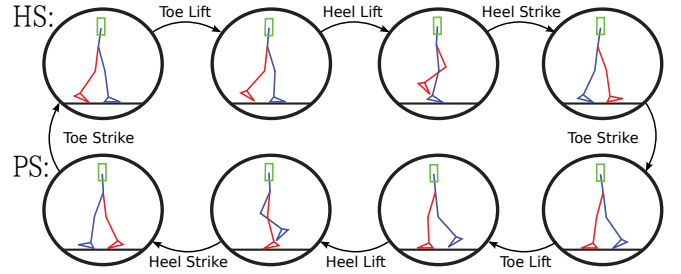


Fig. 3: Two-step domain graph of the asymmetric amputee-prosthesis gait.

Fig. 3. More details of normal multi-domain human locomotion breakdown can be referred to in [4], [32], [33]. With notation  $x = (q; \dot{q})$ , the affine control system for each domain  $\mathcal{D}_v$  can be obtained as  $\dot{x} = f_v(x) + g_v(x)u_v$  by reformulating (3) and (4) [30]. The discrete behavior,  $\Delta_e$ , of impacts is modeled with the assumption of perfectly plastic impacts, i.e., there is no deformation, slippage or bounce of the feet during impacts (details about the impact model can be found in [18], [30]).

### B. Virtual Constraints based Control Law

This section introduces the hybrid zero dynamics (HZD) based virtual constraints framework [2], built upon which a nonlinear optimization-based control law is presented.

**Virtual Constraints.** Analogous to holonomic constraints that are imposed by the physical environment, virtual constraints are defined as a set of functions that modulate the joints of a robot in order to achieve certain desired behavior [30]. In particular, virtual constraints are defined as the difference between the actual and desired outputs of the robot systems:

$$y_{1,v} = y_{1,v}^a(q, \dot{q}) - y_{1,v}^d(\alpha_v), \quad (5)$$

$$y_{2,v} = y_{2,v}^a(q) - y_{2,v}^d(q, \alpha_v), \quad (6)$$

for  $v \in V$ , where  $y_{1,v}$  and  $y_{2,v}$  are relative degree 1 and (vector) relative degree 2 virtual constraints by definition, respectively [25]. Specifically, we assume the desired velocity-modulating outputs to be a constant, i.e.,  $y_{1,v}^d(\alpha_v) = v_d \in \mathbb{R}$  and the desired position-modulating outputs are given in term of a Bézier polynomial of degree  $M$  [15], [30]:

$$y_2^d(\tau, \alpha_o) := \sum_{k=0}^M \alpha_o[k] \frac{M!}{k!(M-k)!} \tau^k (1-\tau)^{M-k}, \quad (7)$$

for all  $o \in \mathcal{O}_v$  with  $\mathcal{O}_v$  be an indexing set of outputs, and  $\alpha_o$  is a vector of Bézier polynomial coefficients. Explicit discussion of the outputs set for each domain is omitted here as the major focus of this work are the ankle and knee joints. Details can be referred to [33], [35].  $\tau$ , the phase variable, which has to be monotonic over a gait cycle, is introduced aiming to create a robust state-feedback controller as discussed in [30]. The end result of introducing the virtual constraints is that the problem of reproducing human-like prosthetic walking reduces to designing and tracking the gait parameters  $v_d$  and  $\alpha_v$ .

**Nonlinear Prosthetic Control Law.** In previous work [34], the authors proposed a novel nonlinear prosthetic controller that combines the *rapidly exponentially stabilizing control Lyapunov functions* (RES-CLFs) based quadratic program control ( $\mu^{qp}$ ) [3] with impedance control ( $\mu^{imp}$ ) in an effort to achieve better tracking and improved energy efficiency on prostheses. This section will introduce this method in a brief way. For more details, we refer the readers to [34].

Applying the human-inspired feedback linearization controller [2], the original affine control system of the prosthetic joints can be converted to a linear form as follows:

$$\dot{\eta} = \underbrace{\begin{bmatrix} 0_{2 \times 2} & I_{2 \times 2} \\ 0_{2 \times 2} & 0_{2 \times 2} \end{bmatrix}}_F \eta + \underbrace{\begin{bmatrix} 0_{2 \times 2} \\ I_{2 \times 2} \end{bmatrix}}_G \mu, \quad (8)$$

where  $\eta = (y_p; \dot{y}_p) \in \mathbb{R}^{4 \times 1}$  with  $y_p$  the virtual constraints for the prosthetic joints. Leveraging the Continuous Algebraic Riccati Equation with solution  $P = P^T > 0$ , allows for the construction of a RES-CLF:  $V_\varepsilon(\eta) = \eta^T \begin{bmatrix} \frac{1}{\varepsilon} I & 0 \\ 0 & I \end{bmatrix} P \begin{bmatrix} \frac{1}{\varepsilon} I & 0 \\ 0 & I \end{bmatrix} \eta := \eta^T P_\varepsilon \eta$  with convergence rate  $\varepsilon > 0$  [3]. In order to exponentially stabilize the system, we want to find  $\mu$  such that, for a chosen  $\gamma > 0$  [3], we have:

$$L_F V_\varepsilon(\eta) + L_G V_\varepsilon(\eta) \mu \leq -\frac{\gamma}{\varepsilon} V_\varepsilon(\eta), \quad (9)$$

where  $L_F V_\varepsilon(\eta)$  and  $L_G V_\varepsilon(\eta)$  are the corresponding Lie derivatives. Since this inequality is affine in  $\mu$ , it can be solved via a quadratic program (QP) to achieve (point-wise) optimal choices of  $\mu^{qp}$ . More importantly, we add the impedance term  $\mu^{imp}$  into the this construction for the total hardware torque bounds, which yields the following model independent quadratic program plus impedance control (MIQP+Impedance):

$$\begin{aligned} & \underset{(\delta, \mu^{qp}(\eta)) \in \mathbb{R}^{2 \times 1}}{\operatorname{argmin}} \quad p\delta^2 + \mu^{qpT} \mu^{qp} & (10) \\ & \text{s.t. } L_F V_\varepsilon(\eta) + \frac{\gamma}{\varepsilon} V_\varepsilon(\eta) + L_G V_\varepsilon(\eta) \mu^{qp} \leq \delta, \quad (\text{CLF}) \\ & \quad \mu^{qp} \leq \mu_{MAX}^{qp}, & (\text{Max QP Torque}) \\ & \quad -\mu^{qp} \leq \mu_{MAX}^{qp}, & (\text{Min QP Torque}) \\ & \quad \mu^{qp} \leq \mu_{MAX} - \mu^{imp}, & (\text{Max Input Torque}) \\ & \quad -\mu^{qp} \leq \mu_{MAX} + \mu^{imp} & (\text{Min Input Torque}) \end{aligned}$$

where  $\delta$  is a relaxation factor that ensures that hardware constraints (related to torque) take priority over control objectives. The total input torque is  $\mu = \mu^{qp} + \mu^{imp}$ . This QP problem yields a model-independent optimal controller that regulates the error in the virtual constraints dynamics in a rapidly exponentially convergence fashion. Simultaneously, by adding the impedance control as a feed-forward term into the input torque, the model independent dynamic system (8) gathers some information about the system that it is controlling. We can also set the torque bounds  $\mu_{MAX}$  such that the optimization-based control law will generate torques that respect the hardware torque bounds (see [34]).

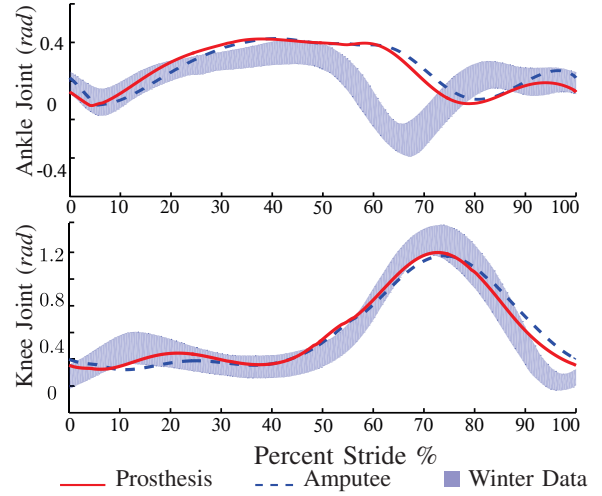


Fig. 4: Trajectory comparisons between the optimized amputee-prosthesis joints and the nominal human locomotion trajectory from Winter data [31].

### C. Two-Step Optimization for Prosthetic Gait Design

As discussed in Sec. II-A, a periodic two-step gait cycle of the amputee-prosthesis walking consists of 8 continuous domains. To efficiently solve such a complicated nonlinear optimization problem, we apply the direct collocation based multi-domain HZD gait design approach introduced in [15] with particular modifications for the two-step hybrid system. Here, we simply introduce the main idea of the direct collocation optimization. In particular, the solution of each domain,  $\mathcal{D}_v$ , is discretized based on the time discretization

$$0 = t_0 < t_1 < t_2 < \dots < t_{N_v} = T_{I,v}, \quad (11)$$

assuming  $T_{I,v} > 0$  is the time at which the system reaches the guard associated with a given domain. Let  $x^i$  and  $\dot{x}^i$  be the approximated states and first order derivatives at node  $i$ , the defect constraints are defined at each odd node as:

$$x^i - 3(x^{i+1} - x^{i-1})/2\Delta t_v^i + (x^{i-1} + x^{i+1})/4 = 0, \quad (12)$$

$$x^i - (x^{i+1} + x^{i-1})/2 - \Delta t_v^i (x^{i-1} - x^{i+1})/8 = 0, \quad (13)$$

where  $\Delta t_v^i = t_{i+1} - t_{i-1}$  is the time interval. Moreover, the first order derivatives must satisfy the system dynamics, i.e.,  $\dot{x}^i = f_v(x^i) + g_v(x^i)u_v^i$ . In particular, the control inputs  $u_v^i$  at each node is enforced to be the feedback linearization controllers discussed in Sec. II-A. Further, the domain admissible constraints and guard condition are also imposed accordingly. The system states between two continuous domains are connected by enforcing the discrete dynamics,  $\Delta_e$ , of each associated edge.

Followed from the general construction of the multi-domain HZD gait optimization in [15], we state the two-step amputee-prosthesis gait optimization to minimize the mechanical Cost of Transport (CoT) of the gait, given as:

$$\underset{\mathbf{z}^*}{\operatorname{argmin}} \quad \Phi_{CoT}(\mathbf{z}) \quad (14)$$

$$\text{s.t. } \mathbf{z}_{\min} \leq \mathbf{z} \leq \mathbf{z}_{\max}, \quad (15)$$

$$\mathbf{c}_{\min} \leq \mathbf{c}(\mathbf{z}) \leq \mathbf{c}_{\max}, \quad (16)$$

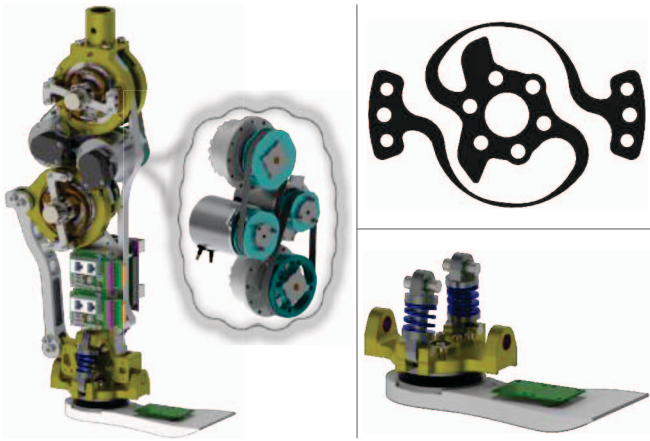


Fig. 5: The novel design features of AMPRO3, including: Transmission (Left), Torsion Springs (top right), and Ankle Roll Joint (bottom right).

where  $\mathbf{z}$  is the set of all decision variables, and  $\mathbf{c}(\mathbf{z})$  is a collection of necessary constraints presented in [15]. Due to the page limit, we omit the detailed construction of the optimization in this paper (see [15] for more details).

In Addition to computational efficiency, another important advantage of the direct collocation optimization formulation is that it allows us to impose various practical and realistic constraints directly, which yields a better designed prosthetic gait. In particular, the constraints we considered include *Human-likeness Constraints*, *Comfortability Constraints* and *Physical Limitation Constraints*. For more specific details about implementation of these constraints, we refer the readers to [32]. The resulting gait after solving this optimization problem can be seen in Fig. 4 with the comparison between the normal human locomotion data from Winter [31].

### III. DESIGN OF AMPRO3

To experimentally validate the systematic control methodology—including hybrid system modeling, nonlinear control and gait generation—a new powered transfemoral prosthesis, AMPRO3, is designed and built from ground up. The mechanical design of AMPRO3 is discussed here with a special focus on the various compliant components. The electrical on-board computation and sensing of AMPRO3 are then illustrated in detail.

#### A. Mechanical Design of AMPRO3

The design of AMPRO3, seen in Fig. 1, provides the convenience of on-board power alongside the advantages of highly dynamic motion and sensing capabilities, all in a compact design. The device weighs in at 5.95 Kg without the knee adapter, and reaches a total height of 451 mm. Both the knee and ankle flexion/extension joints are actuated and actively controlled on this device. A closer look at the transmission drives is shown in Fig. 5. Each of these joints contains a 206 W brushless DC motor (MOOG BN23) capable of just over 1 Nm peak torque. In order to achieve the desired torques associated with human walking, harmonic

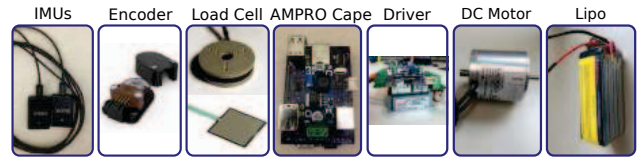


Fig. 6: Electric components of 3D prosthesis AMPRO3.

Gearheads with a 1:100 reduction are placed between the motor and the joint.

Unlike previous AMPRO models, which had the motor and gearhead mounted in line with each other [34], AMPRO3 has the gearhead separated from the motor and then connected via a timing belt. Adding this belt connection between the two allows for separate management of the gear reduction at each joint, while still using the same motors and gearheads for both. The belts are also used to produce the last reduction between the motor and joints. The belt ratio in the ankle and knee transmissions are 4:7 and 5:6, respectively. Table I shows the final gear ratio, peak torque ( $T_p$ ), continuous torque ( $T_c$ ), and max speed ( $V_{max}$ ) for each joint's transmission. The joint torques listed include an approximate efficiency of the harmonic gearheads of 70%. In addition to these changes, two major design changes were made in AMPRO3 from previous versions. These key changes are discussed separately in the following paragraphs.

**SEA Joints.** The first major mechanical design change within AMPRO3 is the addition of compliance at each joint. For the two actuated degrees of freedom, this compliance is represented in the form of a planar torsional spring mounted between the gearhead and the joint. The resulting compliance from the springs decreases the effects of impact on the motors and user, leading to smoother and more comfortable movement. The shape of the torsion springs is based on the design of [19], modified only for mounting purposes and to reach the desired stiffness of 20Nm/deg. The spring model is shown in Fig. 5. The stiffness of these springs was chosen based on the joint torque profile seen in simulation. Adding in this compliance between the motor and the joint creates the possibility of a SEA. In cases like walking, where impacts happen at predictable moments within the gait, it becomes possible to control the timing of energy storage and release in coordination with desired motion, thus saving energy [22].

**Compliant Passive Ankle Roll Joint.** Motivated by the fact that lateral ankle movement plays an important role for a person's preferred motion during walking (for example, walking on uneven terrains) [10], AMPRO3 also contains a third joint, ankle roll, as another major change from previous designs. This joint is not actuated, although motion is passively controlled through compression springs as shown

TABLE I: Joint Transmission Capabilities

Joint	Gear Ratio	$T_p$ (Nm)	$T_c$ (Nm)	$V_{max}$ (rad/s)
Ankle	1:175	123	38.5	4.0
Knee	1:120	85	26.5	5.8

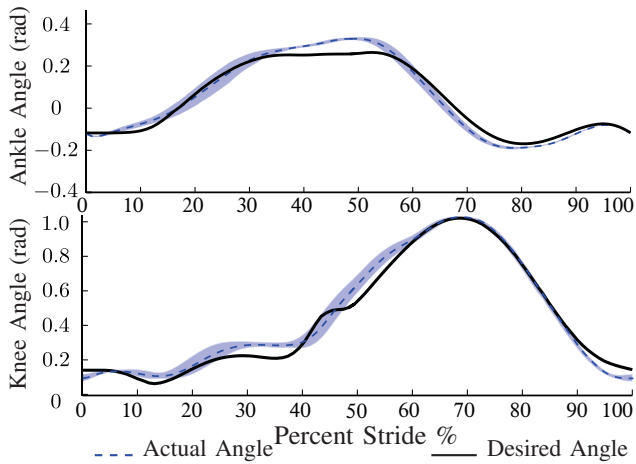


Fig. 7: Averaged experimental joint angles of 3D multi-contact prosthetic walking compared with desired trajectory. Grey area is the corresponding one standard deviation.

in Fig. 5. These springs are linear and placed on both sides of the joint, leading to a roll joint stiffness of about 2.1Nm/deg. The stiffness of these springs was chosen through a control-in-the-loop method of design, as in [24]. The optimization for the prosthetic model was run with multiple spring constants, and the final choice was made based on gait parameters like joint torques and cost of transport.

While the addition of this roll joint provides further compliance between the environment and the user, it also allows for a wider variety of gaits and control methods through available 3D movement [7]. The user can change the width of their stance or walking, and navigate sloped terrain. Based on the designed gaits in simulation, the range of motion for this joint is limited through hard-stops to provide up to 5 degrees of adduction and 2 degrees of abduction. The latter is limited to ensure the user does not move their center of pressure outside their base of support.

### B. On-board Sensing and Computation

A BeagleBone Black (BBB) micro-controller runs the three-level control architecture—including sensing and computation—on board the prosthetic. The low-level control of motor driving comes from two ELMO motion controllers (Gold Solo Whistle). The motion controllers are actively controlling the motion of the ankle and knee joints using feedback from two encoders at each joint and input from the BBB. An incremental encoder placed on the motor side of the joints and an absolute encoder placed on the joint output side can be used to measure any deflection of the torsion spring. User sensory feedback is provided to the device through an Inertial Measurement Unit (IMU) fixed to the knee adapter. Further environment sensing is gained from a 6-axis load cell in the foot. Two flex force sensors can also be mounted at the heel and toe of the foot to provide on-and-off ground contact feedback during more complex foot motion (e.g., multi-contact with heel strike and toe off). The whole system is powered through a 9-cell (33.3 V), 3900 mAh Li-Po battery (ThunderPower).

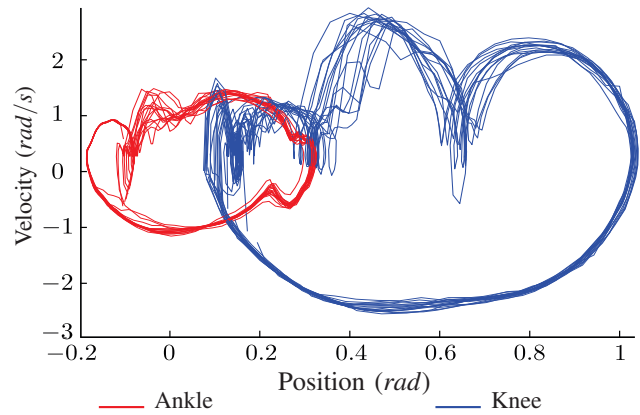


Fig. 8: Phase portraits of the experiment results over 20 steps.

To expand the functionality of the BBB, a custom printed circuit board (PCB): AMPRO Cape, is designed. The Cape adds in a CAN bus chip (for communicating with ELMO drives), 4 USB ports (for communicating with load cell, force sensors and IMUs) and a 5V voltage regulator (for power supply of the BBB and USB ports). For the purpose of better wire organization, we also designed a PCB for the ELMO motion driver. This ELMO board contains a) a voltage converter to power the logic board of the ELMO; and b) serial CAN bus and power connectors to allow multiple ELMOs to be connected in serial. The result is a compactly organized self-contained prosthesis. The major electric components are shown in Fig. 6 and the assembled hardware of AMPRO3 is shown in Fig. 1. The three-level control architecture of AMPRO3 is similar to AMPRO1, which can be referred to [35]. The high level controller of AMPRO3 is coded into C++ packages and runs on the ROS. The detailed discussion is omitted here and can be referred to in the discussion of AMPRO1 [34].

## IV. EXPERIMENTAL VALIDATION

### A. Experiment Setup and Results

Walking trials were performed on a treadmill with a constant speed of 1.4 mph. During the testing, an adapter must be worn between the knee of the user and the knee of the prosthetic to bypass the healthy shank of the unimpaired testing subject. An iWalk 2.0 crutch was modified for this purpose, as seen in Fig. 1. A shoe extension was also necessary to balance the height difference introduced by the knee adapter. Handrails were provided for safety support. Fig. 1 shows the big picture of the experiment setup<sup>1</sup>.

A regular PD controller is implemented first to achieve walking for the purpose of impedance parameter estimation. We then apply impedance control  $\mu^{imp}$  as the feed-forward term while using the MIQP control  $\mu^{qp}$  as the feedback term to track the desired 3D prosthetic gaits, i.e., joint trajectories. The resulting joint trajectories are compared with the designed gait in Fig. 7, showing that the obtained

<sup>1</sup>The experimental protocol has been approved by the Institutional Review Board (IRB) at the Georgia Institute of Technology.

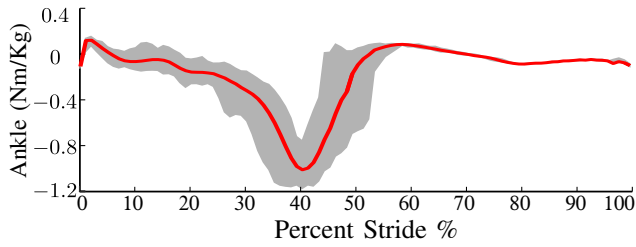


Fig. 9: Normalized experimental ankle torque of the 3D multi-contact prosthetic walking. Grey area is the boundary of the experiment results over 20 steps.

prosthetic walking is able to realize the designed gait successfully and shares a similar pattern as the healthy human locomotion, which can be referred to in Fig. 4. The phase portraits of both joints are shown in Fig. 8. With a particular interest of the foot push behavior, the average torque of the ankle pitch joint is provided in Fig. 9. Experiment gait tiles of the multi-contact level-ground walking using the proposed optimization-based controller along with the simulated 3D prosthetic walking are shown in Fig. 10. We also took AMPRO3 on a trip to Washington DC for a live demonstration at an NRI-sponsored event. The device was successfully demonstrated in both outdoor and indoor environments in DC. A video [1] is attached which shows both the experimental multi-contact walking and outdoor walking demonstration.

### B. Discussion

For the preliminary testings, we neglect the effects of the torsional springs during the control and tracking. Only the incremental encoder is considered for each joint. Therefore, because of the compliant effect of the torsional springs between the joint and the motor, the tracking results, shown in Fig. 7, are not as good as the case of AMPRO1 [34], which used a rigid chain drive. More sophisticated SEA control will be a future research topic as an extension of this work. The torque profile of the ankle joint in Fig. 9 clearly indicates a foot push at the end of the stance phase, which is an essential character for natural multi-contact human walking. Note that, the foot push is also reported by the user, which is lacking during the flat-foot style walking [34]. Therefore, we can conclude that AMPRO3 has achieved realistic human-like walking both kinematically and kinetically.

With a particular interest in the power performance of AMPRO3, the average one-step power consumption of AMPRO3 (over 20 steps) is compared with both AMPRO1 and the Vanderbilt Leg [27] in Fig. 11. Note that, due to the limitation of the sensory capability of AMPRO3, only mechanical power can be calculated, i.e., we use the joint torque times velocity for power estimation. Since both the BBB and ELMO have fairly low power consumption during one step (0.8 s duration), these two terms will not affect the total power figure significantly. The test subjects for AMPRO1 and AMPRO3 are also slightly different (160 lb for AMPRO1 vs 155 lb for AMPRO3). We realize these limitation for the preliminary results. Future work will improve

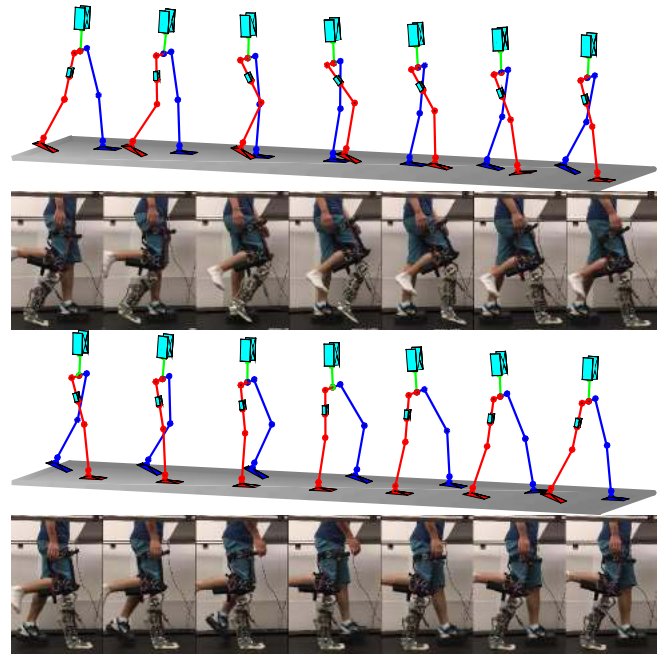


Fig. 10: AMPRO3 Gait tile comparison between the experimental walking and the simulated walking.

the power estimation by considering the power consumed by the electronic components. More testing subjects will also be considered. From the estimated power comparison of the preliminary experiments, we can see that the proposed optimization-based controller outperforms both the traditional controller and the Vanderbilt Leg. More importantly, AMPRO3 consumes much less energy than AMPRO1. The possible reasons are threefold: a) AMPRO3 is lighter and smaller than AMPRO1; b) The tracking of AMPRO3 is not as good as AMPRO1; therefore, less energy is required; c) the passive springs in the system can help store and release energy.

## V. CONCLUSIONS

This work presented the preliminary experiment results of 3D multi-contact prosthetic walking via extending the systematic methodology from 2D case of AMPRO1 to the 3D case of AMPRO3. With a 3D asymmetric hybrid system model, a more realistic amputee-prosthesis model with compliance was constructed. Based on this model, a two-step direct collocation optimization method was developed to design natural 3D multi-contact prosthetic gaits, which satisfy various practical constraints. Cost of Transport was used as the objective function with the goal of achieving more energy efficient gaits.

A novel 3D compliant powered prosthesis, AMPRO3, was designed and built to experimentally validate this approach. Detailed system design of AMPRO3 including two SEA joints and one passive compliant ankle roll joint were discussed explicitly. For the preliminary testings, the resulting 3D prosthetic walking was energy efficient while at the same time displaying natural multi-contact features with significant foot push. While the focus of this work was to

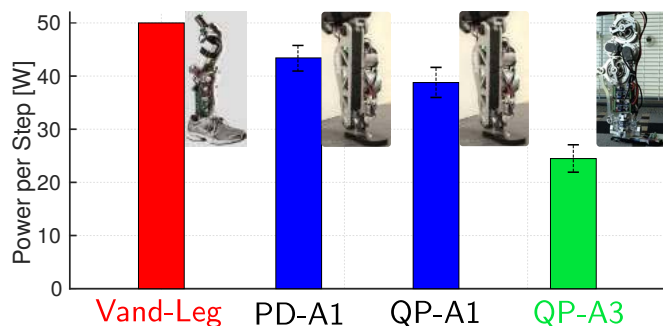


Fig. 11: Power comparison of natural multi-contact prosthetic walking among Vanderbilt Leg (Vand-Leg) with impedance control [27], AMPRO1 & 3. PD-A1 and QP-A1 are PD+Impedance and MIQP+Impedance with AMPRO1, respectively [35]; QP-A3 is MIQP+Impedance with AMPRO3.

introduce the system design and initial testings of AMPRO3, the preliminary results, along with these novel hardware improvements, opened the door for compliant joint control with energy saving and amputee comfortability. Future work will be focused on the control of SEA joints and clinical testings on real amputees.

#### REFERENCES

[1] 3D multi-contact walking of AMPRO3. <https://youtu.be/496xsYxGuV8>.

[2] A. D. Ames. Human-inspired control of bipedal walking robots. *Automatic Control, IEEE Transactions on*, 59(5):1115–1130, 2014.

[3] A. D. Ames, K. Galloway, K. Sreenath, and J. W. Grizzle. Rapidly exponentially stabilizing control lyapunov functions and hybrid zero dynamics. *Automatic Control, IEEE Transactions on*, 59(4):876–891, 2014.

[4] A. D. Ames, R. Vasudevan, and R. Bajcsy. Human-data based cost of bipedal robotic walking. In *Hybrid Systems: Computation and Control*, pages 153–162, Chicago, IL, 2011.

[5] S. Au, M. Berniker, and H. Herr. Powered ankle-foot prosthesis to assist level-ground and stair-descent gaits. *Neural Networks*, 21(4):654–666, 2008.

[6] V. Azimi, D. Simon, H. Richter, and S. A. Fakoorian. Robust composite adaptive transfemoral prosthesis control with non-scalar boundary layer trajectories. In *American Control Conference*, 2016.

[7] C. E. Bauby and A. D. Kuo. Active control of lateral balance in human walking. *Journal of Biomechanics*, 33(11):1433–1440, 2000.

[8] J. Casillas, V. Dulieu, M. Cohen, I. Mercer, and J. Didier. Bioenergetic comparison of a new energy-storing foot and sach foot in traumatic below-knee vascular amputations. *Archives of physical medicine and rehabilitation*, 76(1):39–44, 1995.

[9] T. Dillingham. Limb amputation and limb deficiency: Epidemiology and recent trends in the united states. *Southern Medical Journal*, 2002.

[10] E. Ficanha, M Rastgaar, and K. Kaufman. A two-axis cable-driven ankle-foot mechanism. *Robotics and Biomimetics*, 1(17), 2014.

[11] R. D. Gregg, T. Lenzi, L. J. Hargrove, and J. W. Sensinger. Virtual constraint control of a powered prosthetic leg: From simulation to experiments with transfemoral amputees. *Robotics, IEEE Transactions on*, 30(6):1455–1471, 2014.

[12] J. W. Grizzle, C. Chevallereau, R. W. Sinnet, and A. D. Ames. Models, feedback control, and open problems of 3d bipedal robotic walking. *Automatica*, 50(8):1955–1988, 2014.

[13] A. Gunnar and L. Peterson. Effects of shoe and surface characteristics on lower limb injuries in sports. *Journal of Applied Biomechanics*, 2(3):202–9, 1986.

[14] K. A. Hamed and R. D. Gregg. Decentralized feedback controllers for exponential stabilization of hybrid periodic orbits: Application to robotic walking\*. In *American Control Conference*, pages 4793–4800, Boston, 2016.

[15] A. Hereid, E. A. Cousineau, C. M. Hubicki, and A. D. Ames. 3d dynamic walking with underactuated humanoid robots: A direct collocation framework for optimizing hybrid zero dynamics. In *Robotics and Automation (ICRA), 2016 IEEE International Conference on*, pages 1447–1454. IEEE, 2016.

[16] J. K. Hitt, T. G. Sugar, M. Holgate, and R. Bellman. An active foot-ankle prosthesis with biomechanical energy regeneration. *Journal of medical devices*, 4(1):011003, 2010.

[17] K. W. Hollander and T. G. Sugar. A robust control concept for robotic ankle gait assistance. In *Rehabilitation Robotics, ICORR, IEEE 10th International Conference on*, pages 119–123, 2007.

[18] Y. Hürmüzlü and D. B. Marghitu. Rigid body collisions of planar kinematic chains with multiple contact points. *Intl. J. of Robotics Research*, 13(1):82–92, February 1994.

[19] C. A. Ihrke, A. H. Parsons, J. S. Mehling, and B. K. Griffith. Planar torsion spring, US 20100145510. June 2010.

[20] J. F. Lehmann, R. Price, S. Boswell-Bessette, A. Dralle, K. Ques-tad, and B. J. DeLateur. Comprehensive analysis of energy storing prosthetic feet: Flex foot and seattle foot versus standard sach foot. *Archives of physical medicine and rehabilitation*, 74(11):1225–1231, 1993.

[21] R. M. Murray, Z. Li, and S. S. Sastry. *A Mathematical Introduction to Robotic Manipulation*. CRC Press, Boca Raton, March 1994.

[22] D. Paluska and H. Herr. The effect of series elasticity on actuator power and work output: Implications for robotic and prosthetic joint design. *Robotics and Autonomous Systems*, 54(8):667–673, 2006.

[23] K. Postema, H. J. Hermens, J. De Vries, H. Koopman, and W. H. Eisma. Energy storage and release of prosthetic feet part 1: Biomechanical analysis related to user benefits. *Prosthetics and Orthotics International*, 21(1):17–27, 1997.

[24] J. Reher, E. A. Cousineau, A. Hereid, C. M. Hubicki, and A. D. Ames. Realizing dynamic and efficient bipedal locomotion on the humanoid robot durus. In *International Conference on Robotics and Automation (ICRA)*, pages 1794–1801. IEEE, 2016.

[25] S. S. Sastry. *Nonlinear Systems: Analysis, Stability and Control*. Springer, New York, June 1999.

[26] A. M. Simon, K. A. Ingraham, N. P. Fey, S. B. Finucane, R. D. Lipschutz, A. J. Young, and L. J. Hargrove. Configuring a powered knee and ankle prosthesis for transfemoral amputees within five specific ambulation modes. *PloS one*, 9(6):e99387, 2014.

[27] F. Sup, A. Bohara, and M. Goldfarb. Design and Control of a Powered Transfemoral Prosthesis. *The International journal of robotics research*, 27(2):263–273, February 2008.

[28] L. Torburn, J. Perry, E. Ayyappa, and S. L. Shanfield. Below-knee amputee gait with dynamic elastic response prosthetic feet: a pilot study. *J Rehabil Res Dev*, 27(4):369–84, 1990.

[29] M. R. Tucker, . Olivier, A. Pagel, H. Bleuler, M. Bouri, O. Lamberg, J. del R Millán, R. Riener, H. Vallery, and R. Gassert. Control strategies for active lower extremity prosthetics and orthotics: a review. *Journal of neuroengineering and rehabilitation*, 12(1):1, 2015.

[30] E. R. Westervelt, J. W. Grizzle, C. Chevallereau, J. H. Choi, and B. Morris. *Feedback Control of Dynamic Bipedal Robot Locomotion*. CRC Press, Boca Raton, June 2007.

[31] D. A. Winter. *Biomechanics and Motor Control of Human Movement*. Wiley-Interscience, New York, 2 edition, May 1990.

[32] H. Zhao, A. Hereid, E. Ambrose, and A. D. Ames. 3D multi-contact gait design for prostheses: Hybrid system models, virtual constraints and two-step direct collocation. In *Decision and Control (CDC), 2016 IEEE 55th Conference on*, pages 3668–3674. IEEE, 2016.

[33] H. Zhao, A. Hereid, W-L Ma, and A. D. Ames. Multi-contact bipedal robotic locomotion. *Robotica*, pages 1–35, 2015.

[34] H. Zhao, J. Horn, J. Reher, V. Paredes, and A. D. Ames. First steps toward translating robotic walking to prostheses: a nonlinear optimization based control approach. *Autonomous Robots*, pages 1–18, 2016.

[35] H. Zhao, J. Horn, J. Reher, V. Paredes, and A. D. Ames. Multicontact locomotion on transfemoral prostheses via hybrid system models and optimization-based control. *IEEE Transactions on Automation Science and Engineering*, 13(2):502–513, 2016.

[36] K. Ziegler-Graham, E. J. MacKenzie, P. L. Ephraim, T. G. Travison, and R. Brookmeyer. Estimating the prevalence of limb loss in the united states: 2005 to 2050. *Archives of physical medicine and rehabilitation*, 89(3):422–429, 2008.